Int. J. Heat Mass Transfer. Vol. 21, pp. 1241–1249
© Pergamon Press Ltd. 1978. Printed in Great Britain
0017-9310/78/0901-1241 $02.00/0

SURFACE TENSION EFFECTS IN HEAT TRANSFER THROUGH THIN LIQUID FILMS

THOMAS E. HINKEBEIN* and JOHN C. BERG†
Department of Chemical Engineering BF-10, University of Washington, Seattle, WA 98195, U.S.A.

(*Received* 9 *November* 1977 *and in revised form* 25 *January* 1978)

Abstract—Heat-transfer data for pools of a pure silicone oil of depths ranging from approximately one millimeter to one centimeter heated from below are presented. Pronounced enhancement of the heat-transfer rate due to surface tension driven convection is found. A theory based on the Stuart power integral technique accurately predicts the experimental results for Nusselt numbers less than two.

NOMENCLATURE

$A, B,$ dimensionless amplitude factors defined in equations (1), (2);
$C_p,$ heat capacity;
$d,$ pool depth;
$g,$ acceleration of gravity;
$h,$ heat-transfer coefficient;
$k,$ thermal conductivity;
$\mathbf{n},$ unit normal to surface;
$p,$ pressure;
$p_0,$ reference pressure;
$\hat{p},$ dimensionless pressure, $d^2p/\mu\kappa$;
$q,$ heat flux;
$s,$ surface area;
$t,$ time;
$\hat{t},$ dimensionless time, $\kappa t/d^2$;
$T,$ temperature;
$\Delta T,$ temperature drop;
$\hat{T},$ dimensionless temperature, $-T/\Delta T$;
$u, v, w,$ velocity components in x, y, z directions;
$\hat{u}, \hat{v}, \hat{w},$ dimensionless velocity components, du/κ, dv/κ, dw/κ;
$\mathbf{v},$ vector velocity;
$\hat{\mathbf{v}},$ dimensionless vector velocity, $d\mathbf{v}/\kappa$;
$x, y,$ horizontal coordinates;
$z,$ vertical coordinate;
$\hat{x}, \hat{y}, \hat{z},$ dimensionless coordinates, x/d, y/d, z/d.

Greek symbols

$\beta,$ vertical temperature gradient;
$\gamma,$ thermal expansivity;
$\kappa,$ thermal diffusivity;
$\mu,$ viscosity;
$\nu,$ kinematic viscosity;
$\rho,$ density;
$\sigma,$ surface tension.

Dimensionless groups

$Bi,$ Biot number, $h_a d/k_a$;
$Ma,$ Marangoni number, $-(d\sigma/dT)_0 \Delta T\, d/\kappa\mu$;
$Nu,$ Nusselt number, $h\,d/k$;
$Pr,$ Prandtl number, ν/κ;
$Ra,$ Rayleigh number, $g\gamma\Delta T\, d^3/\kappa\nu$.

Subscripts

$a,$ value in air above pool;
$c,$ critical value;
$m,$ vertical average;
$0,$ reference state.

Superscripts

$'$, fluctuation quantity;
$\bar{}$, horizontal average;
$t,$ transpose.

INTRODUCTION

MUCH has been published concerning natural convection in shallow pools or films of liquid heated from below, but most studies have focussed either on the theoretical prediction of stability criteria for initially quiescent systems [1–5] or on descriptions of the observed morphology of the flows which result when stability criteria are exceeded [6–8]. Relatively little attention has been given to the convective heat-transfer characteristics of such systems and in particular to the role that surface tension forces play in the convection. While both surface tension and buoyancy forces are responsible for initiating and sustaining the convection, it is surface tension that plays the dominant role when the pool is very shallow, for most liquids less than 1 mm in depth.

Heat-transfer studies concerning pools of the above type appear to be limited to the following. Somerscales and Dropkin [9] compared temperature profiles in turbulent convecting pools with theoretical predictions of Howard [10] and Kraichnan [11], but the latter studies failed to account for surface tension effects. Moreover, vertical heat fluxes were not measured, so that experimental heat-transfer coefficients could not be evaluated. Cabelli and Davis [12] made a thorough numerical study of cellular convection in shallow pools considering the combined effects of buoyancy and surface tension. Although restricted to

*Currently with Sandia Laboratories, Albuquerque, NM.
†To whom correspondence should be addressed.

perhaps unrealistically high heat-transfer coefficients in the air layer above the pool, the study demonstrates the importance of surface tension effects in augmenting the convective heat flux.

Natural convection in thin layers heated from below generally assumes a cellular or quasi-cellular form, as described by Bénard [6], with warm fluid rising at the cell centers, spreading radially outward and cooling at the free upper surface of the cell and finally returning downward as cooled liquid along the cell borders. The surface tension mechanism for sustaining such flow, i.e. the well-known Marangoni effect, depends on the positive gradient of surface tension from cell center to cell border which is inversely proportional to the surface temperature gradient. These surface forces work in concert with buoyancy forces which assist the warm fluid in rising at the cell centers and the cooler fluid in sinking along the cell boundaries. When an additional component is present in the liquid pool there exists the possibility of setting up surface concentration as well as temperature gradients, both of which contribute to the surface tension gradient and hence to the natural convection. Convective heat transfer in solute-bearing pools is treated in a second paper.

The purpose of the present study is to obtain convective heat-transfer data for pure shallow liquid pools heated from below and to provide an analysis capable of describing the above experimental results in particular and of predicting surface tension effects in convective heat transfer in such systems in general. Both the experimental and analytical studies are limited to the laminar convective regime(s) corresponding to moderately super-critical conditions. The experimental results are best described in the context of parameters defined in the analytical model. We thus begin with a consideration of the theoretical analysis.

THEORETICAL ANALYSIS

Determination of a steady state flow field corresponding to moderately post-critical conditions is effected using the "power integral" technique first proposed by Stuart [13–14]. The technique makes use of the form of the velocity and temperature profiles generated in the linear stability analysis, i.e. the profiles corresponding to the neutrally stable condition appropriate to the given system. Stability analyses of adequate generality for surface tension and surface tension–buoyancy initiated convection are presently available in the literature [1–3]. The amplitudes are then determined by requiring that the resulting statistically steady finite amplitude flow satisfies the spatially averaged thermal and mechanical energy balances. The power integral technique is expected to be applicable only in the low heat flux range, where the assumption concerning the form of the flow field should be good. The method was successfully applied by Malkus and Veronis [15] to describe heat convection in super-critical horizontal fluid layers confined between rigid conducting surfaces. The present work extends this analysis to systems with a free upper surface subject to surface tension forces which in turn depend upon the surface temperature distribution. The system under study is a shallow horizontal layer of non-volatile, Newtonian, incompressible liquid infinite in horizontal extent, bounded at the bottom by a solid surface and at the top by an inviscid medium. Both bounding surfaces are assumed to remain flat.

The power integral technique begins by setting the dimensionless z-dependent factors of the velocity and temperature profiles equal to multiples of the corresponding stability analysis profile factors, viz.

$$\hat{\mathbf{v}} = A\hat{\mathbf{v}}_c \text{ and} \tag{1}$$

$$\hat{T} = B\hat{T}_c, \tag{2}$$

where the amplitude coefficients A and B, to be determined by substitution into the averaged thermal and mechanical energy equations, are constants. For pure liquids, instability always sets in via the stationary mode, so that in what follows, only the stationary flow situation is considered.

The solutions for $\mathbf{v}_c$ and T_c from stability analyses are not unique in that several plan form structures are consistent with the linearized differential equations and boundary conditions. The preferred cell shape is believed to be that which corresponds to the maximum rate of heat transport [15], although the difference between the various shapes in this regard is slight. For simplicity, the two-dimensional roll cell structure is assumed in the present analysis.

The spatially averaged steady state form of the thermal and mechanical energy equations appropriate to the system of two dimensional roll cells are, in dimensional coordinates:

$$0 = \frac{\beta}{\beta m}(\hat{w}'\hat{T}')_m + (\overline{\nabla\hat{T}'\cdot\nabla\hat{T}'})_m - \left(\hat{T}'\frac{\partial\hat{T}'}{\partial\hat{z}}\right)_{\hat{z}=1} \tag{3}$$

and

$$0 = Ra(\hat{w}'\hat{T}')_m + [\overline{(\nabla\hat{\mathbf{v}}')\cdot(\nabla\hat{\mathbf{v}}')^t}]_m - \left(\hat{u}'\frac{\partial\hat{u}'}{\partial\hat{z}}\right)_{\hat{z}=1} \tag{4}$$

Equations (3) and (4) are derived in Appendix 1.

The last term in equation (3) vanishes in the limit of very small or very large Biot numbers. This may be seen by considering the thermal boundary condition at the free surface.

$$-k\frac{\partial T}{\partial z} = h_a(T - T_a). \tag{5}$$

After this equation is written in terms of disturbance quantities and is non-dimensionalized, there results:

$$\frac{\partial\hat{T}'}{\partial\hat{z}} = -Bi\,\hat{T}'. \tag{6}$$

If both sides of equation (6) are multiplied by $\hat{T}'$, and the horizontal average is considered, then

$$\left(\hat{T}'\frac{\partial\hat{T}'}{\partial\hat{z}}\right)_{\hat{z}=1} = -Bi(\hat{T}'^2)_{\hat{z}=1}, \tag{7}$$

where the left side of (7) is identical to the last term of equation (3). In the more usual case, as Bi approaches zero, $\hat{T}'$ remains bounded so that the last term in

equation (3) becomes very small. Similarly, as Bi becomes large, $\partial \hat{T}/\partial z$ is bounded while $\hat{T}$ approaches zero, and again the last term in equation (3) becomes small.

Equation (4) balances the rate of conversion of potential energy into kinetic energy by convection against its rate of dissipation by viscosity in the bulk and at the upper surface. The last term is zero for the case of a fixed upper boundary as well as for a hydrodynamically free upper surface if surface tension forces are neglected. When surface tension forces are included, however, as in the present analysis, the last term of equation (4) may be interpreted by considering the shear stress boundary condition at the flat liquid–air interface in two-dimensional flow,

$$\mu\left(\frac{\partial u'}{\partial z}\right)=\frac{\partial \sigma}{\partial x}. \tag{8}$$

The surface tension gradient is balanced by the viscous forces in the underlying fluid. In this case of clean liquid pools, surface tension gradients arise only from temperature variations so that (8) may be written as:

$$\mu\frac{\partial u'}{\partial z}=\left(\frac{\partial \sigma}{\partial T}\right)\frac{\partial T}{\partial x}. \tag{9}$$

If this equation is nondimensionalized, multiplied by the velocity at the free interface, and horizontally averaged, there results

$$\left(\overline{\hat{u}'\frac{\partial \hat{u}'}{\partial \hat{z}}}\right)_{\hat{z}=1}=Ma\left(\overline{\hat{u}'\frac{\partial \hat{T}}{\partial \hat{x}}}\right)_{\hat{z}=1}. \tag{10}$$

The LHS of equation (10) is identical to the last term of equation (4). The Marangoni number, Ma, is a ratio of surface tension to viscous forces, and its magnitude determines the importance of surface tension driven convection.

In the application of the power integral technique to the Marangoni convection problem, it is to be expected that the results will be confined to small amplitude flows, i.e. to the low super-critical Rayleigh and Marangoni numbers. In their analysis of the buoyancy driven convection process, Malkus and Veronis [15] predicted the heat flux to within 15% of the experimental value at ten times the critical Rayleigh number. Similar accuracy should be obtainable for the surface tension driven convection problem. At larger Rayleigh numbers, distortion of the velocity and temperature profiles away from those given by the linear stability analysis becomes significant as nonlinear convective modes further augment heat transfer. This model thus provides a lower bound to the heat-transfer coefficient in its dependence on the Rayleigh number and Marangoni number.

The stability analysis profiles of Palmer [2] are used, and the derivation of the amplitude coefficients for the velocity and temperature fields is given in Appendix 2.

Once the actual velocity and temperature profiles are determined, the vertical heat flux, q, is determined by integrating the thermal energy equation (15), at steady state yielding:

$$q=k\beta_m+\rho C_p(\overline{w'T'})_m. \tag{11}$$

Defining the Nusselt number in the usual way: $Nu = hd/k$; substituting equations (1) and (2) and nondimensionalizing gives:

$$Nu=1-(\overline{\hat{w}_c'\hat{T}_c})_m AB. \tag{12}$$

Upon substitution of the amplitude coefficients, as shown in Appendix 2, we obtain:

$$Nu=1+\frac{1-\dfrac{Ra_c}{Ra}}{\left[\dfrac{(\overline{\hat{w}_c'\hat{T}_c'^2})_m}{(\overline{\hat{w}_c'\hat{T}_c'})_m^2}-1\right]}. \tag{13}$$

The Nusselt number has thus been expressed as a function of the actual system Rayleigh number and quantities obtainable solely from the relevant linear stability analysis. Surface tension effects influence the Nusselt number principally by determining the value of the critical Rayleigh number, Ra_c. The larger the system Marangoni number, the smaller is Ra_c. Secondarily, surface tension gradients influence the shape of the velocity and temperature fields under conditions of neutral stability. Figure 1 shows plots of equation (13) for the important case of zero Biot number at the upper surface (i.e. constant heat flux) and constant temperature at the lower surface and in which the effect of the Marangoni number is displayed explicitly. A Marangoni number of zero corresponds to purely buoyancy driven convection, convection which does not ensue until the critical value of the Rayleigh number (for this case, 669) is exceeded. As an example, a 1 mm deep pool of pure water with an average temperature of 20°C and supporting a temperature drop of 0.1°C, would have an Ra of 1.41 and would thus be stagnant (with a Nu of unity) if buoyancy forces alone were responsible for natural convection. The Marangoni number for the above case, however, is 111, leading to natural convection sustained by a combination of surface tension and buoyancy forces, the former playing the dominant role.* The resulting Nu, as given by equation (13), is 1.509. Equation (13) may be expressed in analytical form as:

$$Nu=1+\left[2.029-0.2354\left(\frac{669-Ra}{669}\right)^2\right]\left[1-\frac{669+\dfrac{54.42Ra^2}{(Ra+8.4035Ma)^2}}{Ra+8.4035Ma+0.081348Ra\left(\dfrac{Ra-8.4035Ma}{Ra+8.4035Ma}\right)}\right], \tag{14}$$

*Pools of water are generally sufficiently contaminated, owing to their relatively high surface tension, that they rarely behave as pure component systems with respect to surface tension driven convection [16]. Water is more accurately treated as a dilute solution of a strongly adsorbing solute, as to be reported in a later paper, while the present analysis should be applicable to most pure organic liquids.

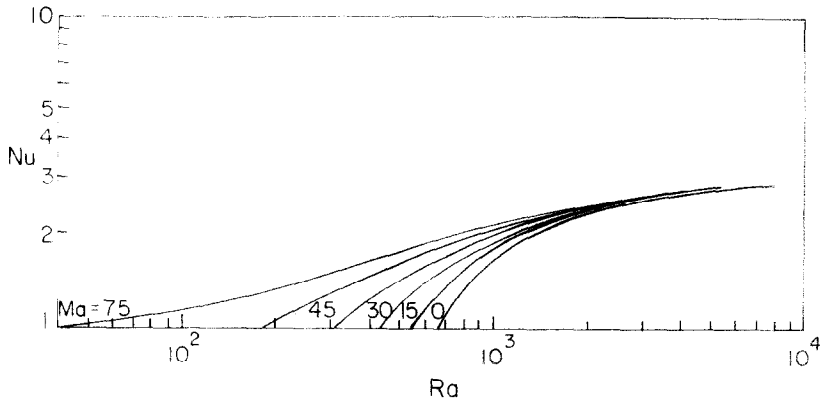

FIG. 1. Computed results for Nusselt number vs Rayleigh number based on equation (13).

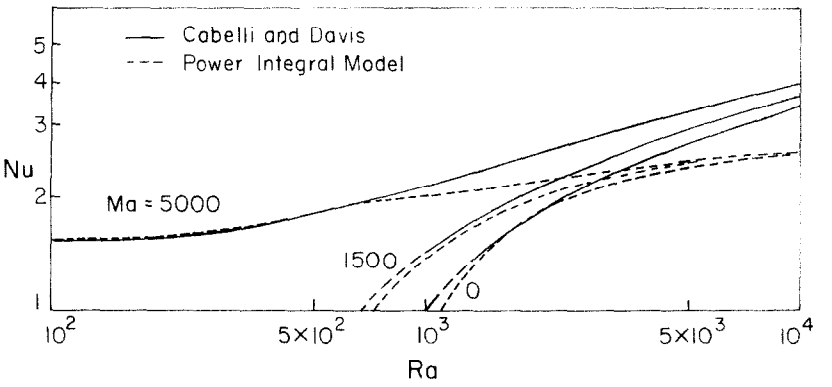

FIG. 2. Comparison of power integral results with computations of Cabelli and Davis [12] for Nusselt number vs Rayleigh number.

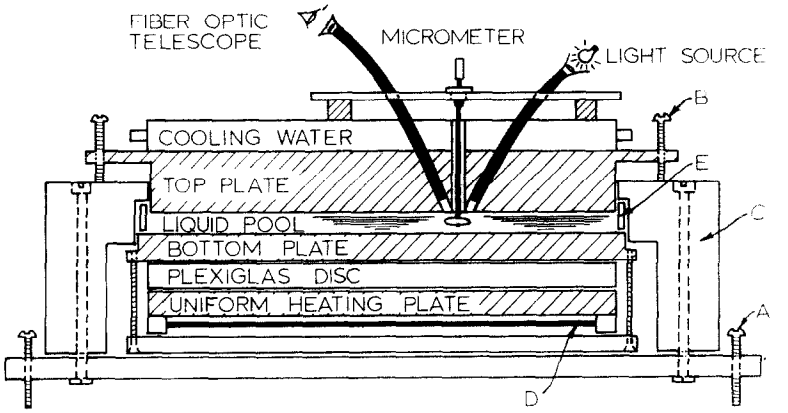

FIG. 3. Schematic diagram of heat-transfer apparatus showing, in addition to labelled items, leveling screws (A), support screws for top plate (B), Plexiglas encasement (C), Nichrome wire heater (D), and Teflon gasket (E).

to within $\pm 0.10\%$ for the case of a constant flux upper surface and constant temperature lower surface. Similar forms may be generated from equation (13) for other thermal boundary conditions at the top and bottom [17].

A comparison of these results with those of Cabelli and Davis (12) is presented in Fig. 2 for the case of a Biot number of 100. Although this unrealistically high Biot number severely depresses the effects of surface tension driven flow, augmentation in the heat flux comparable to those of Fig. 1 for Marangoni numbers two orders of magnitude smaller is observed. It is thus seen that the models agree well up to a Nusselt number of two. At higher heat fluxes Cabelli and Davis' model shows an asymptotic approach to the 1/4 power dependence of *Nu* on *Ra*. The small disagreement at the lower heat fluxes is expected since the Cabelli and Davis calculations near the stability limit are acknowledged to be approximate and do not converge exactly to the linear stability analysis critical limit.

EXPERIMENTAL INVESTIGATION

The apparatus used to make direct measurements of convective heat transfer in shallow pools heated from below is an adaptation of that used by Palmer [18] in detecting the onset of convective instability in such systems and is pictured in vertical cross-section in Fig. 3. The procedure used is sometimes referred to as the Schmidt–Milverton [19] method. Heat flux across the pool is determined as a function of the temperature drop for various liquids and pool depths ranging from approximately 1 to 9 mm. The principal difference between this apparatus and that used in the stability studies, and described in detail there [17, 18], was the addition of a movable thermistor probe with which accurate determinations of free surface temperature could be made. This probe is mounted to a micrometer and positioned with the aid of a fiber optic telescope and light source. The principal components of the heat-transfer apparatus are a 25.4 mm thick aluminum top plate, a 12.7 mm thick aluminum bottom plate, a 9.5 mm thick Plexiglas disk used to monitor heat flux and a second 12.7 mm thick aluminum plate to smooth out lateral temperature nonuniformities from the Nichrome wire heater beneath. The heat-transfer area is circular and 230 mm in diameter. A Teflon gasket provides a seal between the liquid pool and the Plexiglas casing of the apparatus. The entire assembly is encased in Styrofoam insulation to reduce lateral heat losses.

An experimental run begins with the metering of fluid into the apparatus with the top plate removed. The pool is levelled (to within ± 0.02 mm uniform depth), and the top plate assembly is lowered into position by means of support screws until a uniform air gap of 2.0 mm remains above the pool surface. Uniformity of pool and air gap thickness are determined using microscrews. A constant voltage is applied across the Nichrome wire heater, while cooling water maintained at constant temperature to ± 0.01°C is circulated through the baffled cooling water retaining ring atop the upper plate. The apparatus requires 5–10 h to attain steady state as monitored by three copper–constantan thermocouples positioned in the top, bottom and heating plates as well as by a pair of matched thermistors across the calibrated Plexiglas disk. The latter permit the temperature drop across the disk to be measured with an accuracy of ± 0.02°C, which, together with precalibrated lateral heat losses as described in detail elsewhere [18], allow accurate determination of the vertical heat flux through the liquid pool.

The temperature drop across the liquid layer itself is needed for the determination of the heat-transfer coefficient in the pool. This could not be obtained, as in the stability studies, by measuring only the total temperature drop across both air and liquid layers and inferring the liquid surface temperature by assuming the air layer to be stagnant. Although the air layer is always nominally stable under the conditions of the present experiments (the Rayleigh number never exceeds a value of 30, while the critical value is 1708), convective motion in the air is induced by surface movement in the underlying liquid. The liquid surface temperature thus had to be measured directly. Three 3.2 mm dia holes were thus made in the upper plate for positioning and locating a temperature probe in the liquid layer. The hole for the probe itself was drilled normal to the top plate at one-third the distance from the center of the plate to the periphery, while the second and third holes, for a fiber optic light source and telescope, resp., were drilled on angles 30° from the normal and on opposing sides of the first hole. The holes were sufficiently small that they did not disturb the overall uniformity of the upper plate temperature.

The probe is a 0.33 mm bare bead thermistor with a nominal resistance of 8000 Ω at 25°C. The thermistor bead chosen is the smallest economically available so that its presence does not significantly distort the flow field of the liquid and so that it senses as closely as possible a point value rather than a spatially integrated value of temperature. The lead wires are 0.002 mm in diameter and kept in a horizontal plane for approximately 1 cm on each side of the bead, as shown in Fig. 3, to reduce longitudinal heat losses through the leads. The leads are cemented in a hypodermic needle mounted to a micrometer caliper for positioning.

The liquid surface temperature is obtained by locating the temperature probe at various levels within the liquid and extrapolating back to the free surface. Positions are reckoned relative to the free surface, which is located by lowering the probe until it just contacts the liquid as observed through the fiber optic telescope. Since the bottom surface temperature is known from the thermistor permanently located in the bottom plate, the local temperature drop across the liquid layer is defined. The measurement is accurate to within ± 0.07°C. The secondary cooling caused by the probe leads and the hypodermic needle on which the probe is mounted is an important effect and is discussed in more detail below.

Further inquiry into the interpretation of the surface temperature measured by the movable probe must be made because during convection, this temperature varies with horizontal position. The probe of course measures a local value, and it is important to know which value. Since the tip of the hypodermic needle in which the lead wires are mounted closely approaches the free surface and has nearly the temperature of the cold upper plate, it is to be expected that the local liquid surface temperature will be slightly depressed in the vicinity of the probe. This raises the local surface tension and impels the cellular structure to align itself so that the probe is directly above the cold edge of the convecting cell. The surface temperature measured is thus that corresponding to the cold cell boundaries.

Visual confirmation of the cellular structure aligning itself under a cold probe was obtained in separate experiments using schlieren optics. Pools in the absence of the upper plate apparatus were heated from below while a schlieren beam was passed down through the liquid and reflected from the bottom

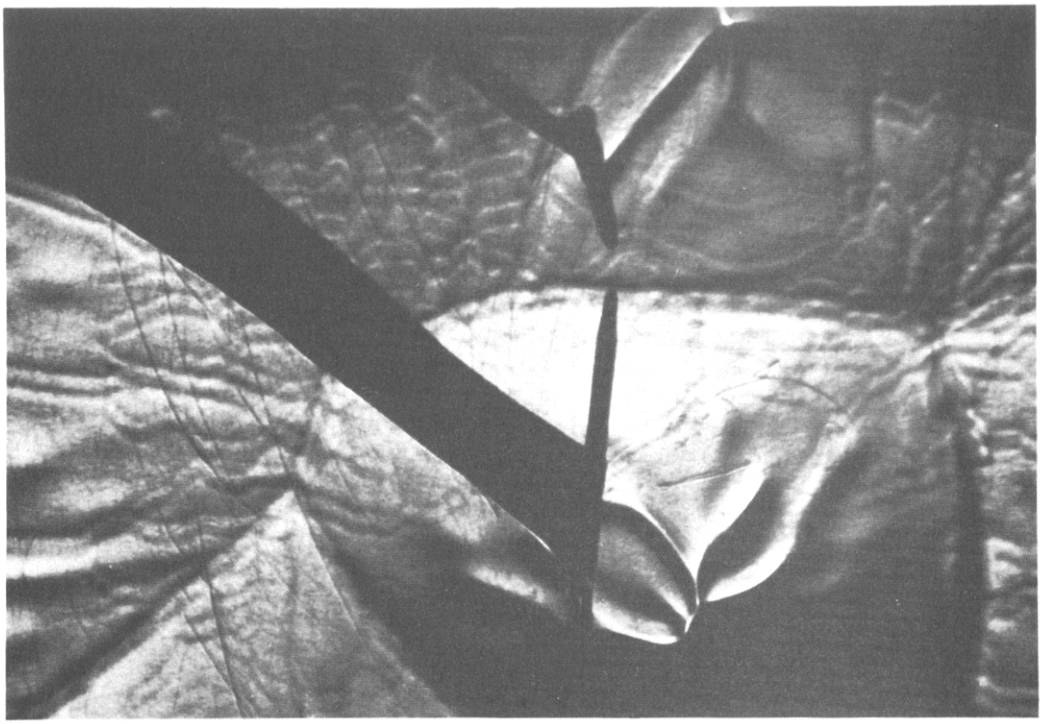

FIG. 4. Schlieren photograph from above of cellular convection in a shallow pool of 10 cs viscosity Dow Corning 200 silicone fluid heater from below. The cold needle shown was initially placed near the cell center, whereupon the cell migrated until the needle tip was above the cell edge. The upper needle image is a reflection. Magnification × 4.

surface revealing the cellular convection, as shown in Fig. 4. In the case shown, a cooled needle was brought near the surface of a pool of 10 cs Dow Corning 200 silicone oil. The initial placement of the needle was directly above the center of the cell. The cell moved until the needle rested directly above the cell boundary, as shown, after which no further migration of the flow structure was observed.

Heat-transfer experiments were performed on 10 cs Dow Corning 200 silicone oil. This liquid was chosen because its extraordinarily low surface tension keeps it free from adsorbed contamination. Its physical properties are summarized in Table 1. Prior to use, the oil was degassed by holding it at 100°C for 1 h. All glassware used for containment of the oil was washed, soaked in Nochromix cleaning solution for 6 h and air dried. The apparatus was disassembled and cleaned prior to each run. The Teflon gasket was soaked in Nochromix, while the aluminum plates were wiped dry with perchloroethylene (an excellent solvent for the silicone oil), washed with soap and water, rinsed liberally with distilled water to remove all traces of soap, and finally flooded with reagent grade absolute ethanol and air dried.

Table 1. Physical properties of Dow Corning 200 10 cs silicone oil at 25°C*

Kinematic viscosity	10 mm^2/s
Specific gravity	0.940
Coefficient of expansion	0.00108 K^{-1}
Thermal conductivity	0.00765 W/m K
Specific heat	101.6 J/kg K
Surface tension	20.1 mN/m
Surface tension–temperature coefficient	−0.068 mN/m K

*Data obtained from Bulletin 05-136 of Dow Corning, Engineering Products Division (1965).

HEAT-TRANSFER RESULTS

The experimental runs covered pool depths ranging from 1.189 to 8.921 mm and therefore embraced the full range of convective behavior from nearly total surface tension dominance, in the shallowest pools, to buoyancy dominance of the convection in the deeper pools. Measurement of heat flux and temperature drop in each case permitted evaluation of the heat transfer coefficient, and results are shown in Fig. 5. In all cases, a stationary steady state was achieved. Of particular importance, the measured temperature drop across the liquid showed no temporal oscillations. As expected, a family of curves of Nusselt number vs Rayleigh number was produced, each member corresponding to a different pool depth. It is noticed that in all runs except those corresponding to the deepest pools, where buoyancy effects strongly predominate, the heat-transfer coefficient is significantly larger than those obtainable if buoyancy effects alone were operative. For the deeper pools, as expected, the Rayleigh number alone is sufficient to correlate the heat transfer data, as indeed the deeper pool data obtained in this study approach a single curve similar to the correlation ov Villarroel [20] for buoyancy driven convection.

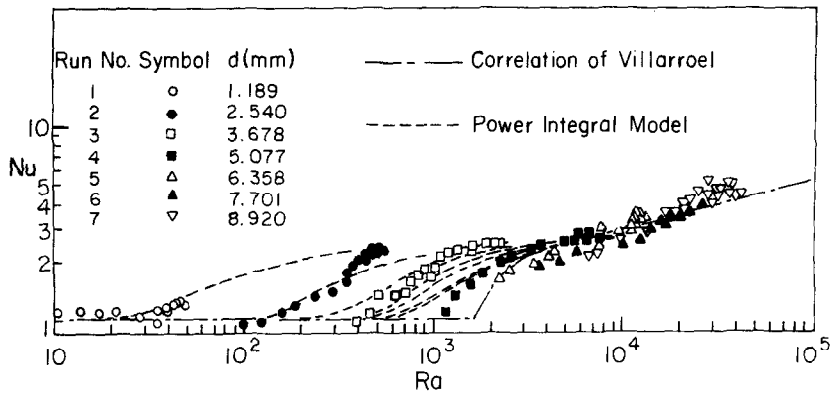

FIG. 5. Plots of experimental data together with predictions of the power integral model (dashed curves).

To make quantitative comparison of the data with power integral theory predictions, it must be recalled that the experimentally measured temperature drop across the liquid is a local value corresponding to the probe being located at the cold edge of the cell. It is thus necessary to calculate the temperature appropriate to the edge of the cell from the power integral model to make a direct comparison of heat-transfer results possible. These computations have been made for all pool depths studied, and the results are shown as dashed lines in Fig. 5. The close similarity between the predicted curves and the experimental data provide reasonable confirmation of the validity of the power integral approach to this problem. Error analysis shows that in all cases but those with higher heat fluxes in the three deepest pools, the differences between the data and the theoretical predictions lie within the error bounds of the data. The upward deviation of the data away from the theoretical curves heralds the expected breakdown of the model as conditions become too far removed from criticality. The theoretical treatment of the convection as though it had a two dimensional roll cell structure rather than the regular polygonal cell structure presumed to exist (and suggested by the auxilliary experiments in which direct observations were made using schlieren optics), appears not to be critical.

We note parenthetically that the data define the stability limit quite accurately. Although the individual heat flux curves are not always observed to rise sharply at the critical temperature gradient, fluid movement which occurs just beyond the stability limit is detectable by a very small amplitude oscillation in the raw temperature data. This oscillation is of the order of 0.001°C so that it does not become apparent in a graphical presentation. The frequency of the oscillation is roughly one cycle per second so that it is easily detectable by this temperature probe which has a 1 s time constant.

CONCLUSIONS

The enhancement of convective heat transfer by surface tension driven natural convection is an important effect in shallow liquid pools heated from below. A modified Schmidt–Milverton technique in which direct measurement of the local fluid interface temperature is possible may be used to obtain quantitative heat transfer data for such systems. The local fluid interface temperature measured will be that corresponding to the cold edge of the convecting cells. A power integral technique, in which the velocity and temperature profiles are set equal to multiples of the relevant profiles corresponding to neutral linear stability, yields equation (13), a predictive equation for the convective heat-transfer coefficient in terms of system parameters and the stability analysis profiles. Results for particular cases are shown in Fig. 1, and equation (14). Heat-transfer data obtained for pools of a 10 cs viscosity silicone oil agree to within experimental uncertainty with the power integral predictions for Rayleigh numbers up to eight times the critical value. For higher degrees of super-criticality the predictions of the heat-transfer coefficient by the power integral technique are low.

Acknowledgement—This work was supported in part by grants from the Office of Saline Water (U.S. Department of the Interior) and the American Society of Heating, Refrigerating and Air-Conditioning Engineers, Inc.

REFERENCES

1. D. A. Nield, Surface tension and buoyancy effects in cellular convection, *J. Fluid Mech.* **19**, 341 (1964).
2. H. J. Palmer and J. C. Berg, Hydrodynamic stability of surfactant solutions heated from below, *J. Fluid Mech.* **51**, 385 (1972).
3. J. R. A. Pearson, On convection cells induced by surface tension, *J. Fluid Mech.* **4**, 489 (1958).
4. A. Pellow and R. V. Southwell, On maintaining convection motion in a fluid layer heated from below, *Proc. R. Soc.* **A176**, 312 (1940).
5. Lord Rayleigh, On convection currents in a horizontal layer of fluid when the higher temperature is on eht lower side, *Phil. Mag., Ser.* 6, **32**, 529 (1916).
6. H. Benard, Les tourbillons cellulaires dans une nappe liquid transportant dc la chaleur par convection en regime permanent, *Annls Chim. Phys.* **23**, 62 (1901).
7. J. C. Berg, M. Boudart and A. Acrivos, Evaporative convection, *Adv. Chem. Engng* **6**, 61 (1966).
8. J. C. Berg, M. Boudart and A. Acrivos, Natural convection in pools of evaporating liquid, *J. Fluid Mech.* **24**, 721 (1966).
9. E. F. C. Somerscales and D. Dropkin, Experimental investigation of the temperature distribution in a hori-

zontal layer of fluid heated from below, *Int. J. Heat Mass Transfer* **9**, 1189 (1966).
10. L. N. Howard, Heat transport by turbulent convection, *J. Fluid Mech.* **17**, 405 (1963).
11. R. H. Kraichnan, Turbulent thermal convection at arbitrary Prandtl number, *Physics Fluids* **5**, 1374 (1962).
12. A. Cabelli and G. D. Davis, A numerical study of the Benard Cell, *J. Fluid Mech.* **45**, 805 (1971).
13. J. T. Stuart, Non-linear effects in hydrodynamic stability, in *Proc. 10th Int. Congr. Appl. Mech. Stresa.*, pp. 63–97. (1960).
14. J. T. Stuart, On the non-linear mechanics of hydrodynamic stability, *J. Fluid Mech.* **4**, 1 (1958).
15. W. V. R. Malkus and G. Veronis, Finite amplitude cellular convection, *J. Fluid Mech.* **4**, 225 (1958).
16. J. C. Berg and A. Acrivos, The effect of surface active agents on convection cells induced by surface tension, *Chem. Engng Sci*, **20**, 737 (1965).
17. T. E. Hinkebein, Surface tension effects in heat transfer through thin liquid films, Ph.D. Dissertation, University of Washington (1976).
18. H. J. Palmer and J. C. Berg, Convective instability in liquid pools heated from below, *J. Fluid Mech.* **47**, 779 (1971).
19. R. J. Schmidt and S. W. Milverton, On the stability of a fluid when heated from below, *Proc. R. Soc.* **A152**, 586 (1935).
20. F. Villarroel, Heat transfer in fluids by Benard convection, M.S. Thesis, University of Maryland (1967).

APPENDIX 1

Derivation of the power integral equations

The coefficients A, B of equations (1) and (2) are determined by requiring the resulting velocity and temperature profiles to be consistent with the spatially averaged thermal and mechanical energy equations (3) and (4), which are derived as follows:

The equation of thermal energy for incompressible flow:

$$\frac{\partial T}{\partial t} + \nabla \cdot \mathbf{v}T - \kappa \nabla^2 T = 0, \tag{15}$$

is averaged over a horizontal plane in the fluid layer to give:

$$\frac{\partial \overline{T}}{\partial t} + \frac{\partial}{\partial z}(\overline{wT}) + \kappa \frac{\partial \beta}{\partial z} = 0, \tag{16}$$

where $\beta = -\partial \overline{T}/\partial z$, the horizontally averaged vertical temperature gradient. Since the precritical steady state velocity is zero, w is simply the perturbation velocity, w', generated by the stability analysis. Primed quantities represent perturbations. The horizontal average of the vertical velocity component vanishes by continuity, so that $\overline{wT}$ in equation (11) may be replaced by $\overline{w'T'}$. Substituting $T = T_0 + T'$ and subtracting equation (16) from (15) then gives:

$$\left(\partial/\partial t - \kappa \nabla^2\right) T' = -\mathbf{v}' \cdot \nabla T' + w'\beta + \frac{\partial}{\partial z}(\overline{w'T'}). \tag{17}$$

Multiplying equation (17) by T' and averaging over the entire fluid yields:

$$\frac{1}{2}\frac{\partial}{\partial t}(\overline{T'^2})_m = \kappa \frac{\iiint T' \nabla^2 T' \, dx\, dy\, dz}{\iiint dx\, dy\, dz} + (\overline{\beta w' T'})_m - \frac{\iiint (T' \mathbf{v}' \cdot \nabla T') \, dx\, dy\, dz}{\iiint dx\, dy\, dz}, \tag{18}$$

where subscript m denotes a vertical average. The last term on the right is easily shown to vanish identically, while the first term on the right may be transformed by Green's theorem to give:

$$\iiint T' \nabla^2 T' \, dx\, dy\, dz = -\iiint \nabla T' \cdot \nabla T' \, dx\, dy\, dz + \iint T' \frac{\partial T'}{\partial n} \, dS, \tag{19}$$

in which the surface integral vanishes everywhere but at the free surface. Substitution of equation (19) into equation (18) gives finally:

$$\frac{1}{2}\frac{\partial}{\partial t}(\overline{T'^2})_m = -\kappa(\overline{\nabla T' \cdot \nabla T'})_m + \frac{\kappa}{d}\left(T' \frac{\partial T'}{\partial z}\right)_{z=d} + (\beta w' T')_m. \tag{20}$$

The averaged mechanical energy equation is derived similarly by taking the inner product of the velocity field with the equation of motion and averaging over the system to yield:

$$\frac{1}{2}\frac{\partial}{\partial t}[\overline{\mathbf{v}' \cdot \mathbf{v}'}]_m = \nu[\overline{\mathbf{v}' \cdot \nabla^2 \mathbf{v}'}]_m - [\overline{\mathbf{v}' \cdot (\mathbf{v}' \cdot \nabla \mathbf{v}')}]_m - \frac{1}{\rho_0}[\overline{\mathbf{v}' \cdot \nabla p}]_m + g\gamma[\overline{w(T - T_0)}]_m. \tag{21}$$

Both the second term and the third term on the right vanish identically. The first term on the right is transformed using Green's theorem:

$$[\overline{\mathbf{v}' \cdot \nabla^2 \mathbf{v}'}]_m = -[\overline{(\nabla \mathbf{v}') \cdot (\nabla \mathbf{v}')}] + \left[\frac{\iint \left(u' \frac{\partial u'}{\partial x} + v' \frac{\partial v'}{\partial y}\right) dx\, dy}{\iint dx\, dy}\right]_{z=d}. \tag{22}$$

where it is noted again that the surface integral on the right vanishes except at the free interface. Substitution of (22) into (21) gives

$$-\frac{1}{2}\frac{\partial}{\partial t}[\overline{\mathbf{v}' \cdot \mathbf{v}'}]_m = -\nu[\overline{(\nabla \mathbf{v}') \cdot (\nabla \mathbf{v}')}]_m + \frac{\nu}{d}\left[u' \frac{\partial u'}{\partial x} + v' \frac{\partial v'}{\partial x}\right]_{z=d} + g\gamma(\overline{w'T'})_m. \tag{23}$$

Nondimensionalization [cf. Nomenclature] of the thermal and mechanical energy equations, i.e. equations (20) and (23) yields:

$$-\frac{1}{2}Pr\frac{\partial}{\partial t}(\overline{\hat{T}'^2})_m = [\overline{\nabla \hat{T}' \cdot \nabla \hat{T}'}]_m - \left[\hat{T}' \frac{\partial \hat{T}'}{\partial \hat{z}}\right]_{\hat{z}=1} + \left[\frac{\beta}{\beta_m} \overline{\hat{w}'\hat{T}'}\right]_m, \tag{24}$$

and

$$-\frac{1}{2}\frac{\partial}{\partial t}(\overline{\hat{\mathbf{v}}' \cdot \hat{\mathbf{v}}'})_m = [\overline{\nabla \hat{\mathbf{v}}' \cdot (\nabla \hat{\mathbf{v}}')'}]_m - \left[\hat{u}' \frac{\partial \hat{u}'}{\partial \hat{z}} + \hat{v}' \frac{\partial \hat{v}'}{\partial \hat{z}}\right]_{\hat{z}=1} + Ra(\overline{\hat{w}'\hat{T}'}), \tag{25}$$

where β_m, the vertically averaged temperature gradient, is obtained by nondimensionalizing and integrating the steady state form of equation (17) on z:

$$\frac{\beta}{\beta_m} = 1 - [(\overline{\hat{w}'\hat{T}'})_m - \overline{\hat{w}'\hat{T}'}]. \tag{26}$$

Finally, applying equations (24) and (25) to the case of stationary two dimensional flow yields equations (3) and (4) in the text.

APPENDIX 2

Derivation of amplitude coefficients and the heat flux relation

If equations (1) and (2) are substituted into spatially averaged thermal energy balance (3), there results

$$0 = \{(1 - AB[(\overline{\hat{w}_c'\hat{T}_c'})_m - (\overline{\hat{w}_c'\hat{T}_c'})]\} AB(\overline{\hat{w}_c'\hat{T}_c'}) + B^2\left\{(\overline{\nabla \hat{T}_c' \cdot \nabla \hat{T}_c'})_m - \left(\hat{T}_c' \frac{\partial \hat{T}_c'}{\partial \hat{z}}\right)_{\hat{z}=1}\right\}. \tag{27}$$

Similarly, the mechanical energy balance, (4), becomes

$$0 = RaAB(\overline{\hat{w}_c'\hat{T}_c'})_m + A^2\left\{(\overline{\nabla\hat{v}_c'\cdot\nabla\hat{v}_c't})_m - \left(\overline{\hat{u}_c'\frac{\partial\hat{u}_c'}{\partial\hat{z}}}\right)_{\hat{z}=1}\right\}. \quad (28)$$

Since all critical velocities and temperatures are known, A and B may be determined as functions of critical parameters and the Rayleigh number. To simplify these equations, the following operational definitions are made:

$$Q_1 = (\overline{\hat{w}_c'\hat{T}_c'})_m \quad (29)$$

$$Q_2 = (\overline{\hat{w}_c'\hat{T}_c'})_m^2 - (\overline{\hat{w}_c'\hat{T}_c'^2})_m \quad (30)$$

$$Q_3 = (\overline{\nabla\hat{T}_c'\cdot\nabla\hat{T}_c'})_m - \left(\overline{\hat{T}_c'\frac{\partial\hat{T}_c'}{\partial\hat{z}}}\right)_{\hat{z}=1} \quad (31)$$

$$Q_4 = [\overline{(\nabla\hat{v}_c')\cdot(\nabla\hat{v}_c')^t}]_m - \left(\overline{\hat{u}_c'\frac{\partial\hat{u}_c'}{\partial\hat{z}}}\right)_{\hat{z}=1} \quad (32)$$

Equations (27) and (28) may now be rewritten.

$$ABQ_1 - A^2B^2Q_2 + B^2Q_3 = 0, \quad (33)$$

and

$$RaABQ_1 + A^2Q_4 = 0. \quad (34)$$

This last equation may be solved for B/A,

$$B/A = -Q_4/(RaQ_1). \quad (35)$$

Equation (35) is substituted into (33) to give

$$AB = \frac{Q_1}{Q_2} - \frac{Q_4Q_3}{Q_1Q_2}\frac{1}{Ra}, \quad (36)$$

where the product AB may be substituted into equation (12) of the text. However, interpretation of (35) is facilitated by considering (27) and (28) at the stability limit where A and B are unity, and Q_2 is much smaller than Q_1, since velocities and temperatures are assumed to have infinitesimal amplitudes at the stability limit. Hence

$$Q_1 = -Q_3 \quad (37)$$

and

$$Ra_c = -Q_4/Q_1. \quad (38)$$

Now AB may be written as

$$AB = \frac{Q_1}{Q_2}\left(1 - \frac{Ra_c}{Ra}\right). \quad (39)$$

Hence equation (12) now may be written

$$Nu = 1 - \frac{Q_1^2}{Q_2}\left(1 - \frac{Ra_c}{Ra}\right). \quad (40)$$

When Q_1 and Q_2 are written in terms of the critical parameters, equation (13) in the text results.

EFFETS DE LA TENSION INTERFACIALE SUR LE TRANSFERT THERMIQUE A TRAVERS DES FILMS MINCES DE LIQUIDE

Résumé—On présente des résultats sur le transfert thermique relatif à l'huile silicone en épaisseur allant d'un millimètre à un centimètre environ. On trouve un accroissement sensible des flux thermiques du à la tension interfaciale. Une théorie basée sur la technique de Stuart prédit correctement les résultats expérimentaux pour des nombres de Nusselt inférieurs à deux.

EINFLUSS DER OBERFLÄCHENSPANNUNG AUF DEN WÄRMEÜBERGANG AN DÜNNEN FLÜSSIGKEITSFILMEN

Zusammenfassung—Es wird über Wärmeübergangsmessungen bei von unten beheizten Behältern mit reinem Silikonöl berichtet. Die Füllhöhe umfaßte einen Bereich von 1 mm bis 1 cm. Es wurde eine deutliche Erhöhung des Wärmeübergangs durch von Oberflächenspannung angeregter Konvektion festgestellt. Mit einer Theorie auf der Grundlage des Potenz-Integral-Ansatzes von Stuary konnten die experimentellen Ergebnisse für Nusselt-Zahlen kleiner als zwei genau wiedergegeben werden.

ВЛИЯНИЕ ПОВЕРХНОСТНОГО НАТЯЖЕНИЯ НА ПЕРЕНОС ТЕПЛА ЧЕРЕЗ ТОНКИЕ ПЛЁНКИ ЖИДКОСТИ

Аннотация — Представлены данные по теплообмену нагреваемого снизу слоя чистого силиконового масла толщиной от одного миллиметра до одного сантиметра. Найдено заметное увеличение скорости передачи тепла в результате действия конвекции, вызванной силами поверхностного натяжения. Экспериментальные результаты для чисел Нуссельта, меньших 2, хорошо обобщаются с помощью интегрального метода Стюарта.